

Photocurrent Distribution across the Interfacial Region of the n-GaAs/Electrolyte Junction

R. Peat, A. R. Kucernak and D. E. Williams[†]

AEA Industrial Technology, Building 552, Harwell Laboratory, Didcot, UK OX11 ORA

A scanning laser microscope has been used to study the photoelectrochemical etching of n-GaAs at the electrolyte interface. Results are presented that show directly, in a qualitative way, the distribution of interfacial charge transfer in the vicinity of microscopic surface defects and the effect of potential and electrolyte composition on this distribution.

Semiconductor electrochemistry is dominated by reference to the ubiquitous surface state. This theoretical formalism appears in many disguises to explain the deviations from ideal behaviour that result from the different types of interactions that occur when the atoms at the surface of a solid interact with the components of an electrolyte phase at a semiconductor/electrolyte junction. This terminology has been used to describe recombination, adsorption, corrosion and phase formation, and yet the physical and chemical nature of the surface state still remains obscure. This obscurity arises in part because traditional electrochemical techniques are macroscopic in the sense that the whole interface is perturbed by some external stimulus and consequently the response induced by the stimulus appears as an average response over the whole surface and any localised information is lost. The surface state is a formal device that describes surface heterogeneity.

Indirect evidence for heterogeneity of the surface is plentiful. The vast literature on wet chemical etches for delineating defects and dislocations from characteristic etch pit patterns testifies to this heterogeneity.^{1,2} These etches generally contain a strong oxidising agent and a complexing species to solubilise the reaction products of the dissolution. The mechanism is considered to be an electrochemical corrosion process in which the oxidising agent is reduced at cathodic surface sites and the substrate is dissolved at the anodic sites. In principle, any external agency which creates electrons and holes will affect the etching rate and illumination has frequently been used.³ Light absorbed in the space-charge region of the solid produces carriers which move to the surface under the influence of the field and consequently photoelectrochemical etching provides an alternative approach to delineate defects under suitable conditions of light intensity, temperature, potential and choice of electrolyte. However, a significant advantage over the chemical etch is that if a focused laser source is used it provides a localised probe and therefore direct information on surface heterogeneity can be obtained at least on the microscopic scale. Photocurrent imaging techniques based on this principle have been developed in recent years.^{4–12}

In this paper a scanning laser imaging technique is used to map the spatial distribution of photocurrent during photocorrosion of the n-GaAs/solution interface. Results are presented that show directly, in a qualitative way, the distribution of interfacial charge

[†] Present address; Department of Chemistry, University College, London, 20 Gordon St, London WC1H 0AJ, UK

transfer in the vicinity of microscopic surface defects and the effect of potential and electrolyte composition on this distribution.

Experimental

The scanning laser microscope has been described in detail elsewhere.¹³ A focused laser spot is rastered over the surface by scanning the light beam using mirrors. Localised photocurrent measurements for each individual beam position are accumulated and then retrieved in the form of a grey-scale image. Photocurrent images can be acquired either directly by measuring the variation of the total current and assuming that the dark current is constant or indirectly by modulation of the light beam combined with phase-sensitive detection techniques to isolate the photocurrent response.¹⁴ The direct method has been used in this study because the photocurrent is large compared with the dark current, and also image acquisition is fast allowing the time evolution of the surface to be studied. The instrument also provides an optical image of the surface that is exactly coincident with the photocurrent image.

Three extra points should be stressed relating to the instrumentation and the form of the image as displayed in this paper. The photocurrent output detected by the potentiostat was d.c. coupled through an amplifier stage and offset to match the incoming signal to the input range of the image processor. The image contrast therefore represents variations in photocurrent across the surface. These variations could be a small fraction of the total photocurrent depending upon the value of the offset compared to the range of the image contrast.

The aspect ratio of the monitor was incompatible with the frame store, so the images are distorted in the vertical direction; *i.e.* a circular electrode would appear as an oval with its long axis in the horizontal direction. While this is inconvenient, it does not alter the general conclusions and value of the results in this paper. Finally, the mode of operation of the mirrors follows a sequence in which the image is created by moving the beam from left to right and top to bottom across a region of the sample. For any particular line, the appropriate mirror scans from left to right and then positions the beam at the beginning of the next sequential line where it waits for a fixed time called the line-blanking period. A similar event occurs at the end of each image frame when the mirrors are moved to deflect the beam to the beginning of the first line of the next frame. The beam is then stationary for a time period called the frame-blanking time. The effect of these blanking periods is that the top left-hand corner of the sample is illuminated throughout the entire frame-blanking time and the left edge of the scanned frame is illuminated for the whole of the line-blanking time. For a material like n-GaAs this extra illumination results in photoetching of the substrate, resulting in a groove corresponding to the left-hand edge and a circular pit at the top left-hand corner of the imaged region. These features are also visible on some of the scanning electron micrographs presented below. The problem has been resolved in later studies by incorporating a shutter to attenuate the laser intensity severely during the line- and frame-blanking cycles.

The n-GaAs electrodes were cut from tin-doped single-crystal wafers in the <100> orientation with a donor density of $1.3 \times 10^{17} \text{ cm}^{-3}$. The material was pulled from the melt using a Czochralski growth apparatus. An ohmic metal contact was prepared using indium solder. The sample was initially polished to a mirror finish with 10, 6, 4 and 1 μm diamond grits followed by slurries of 1 and 0.05 μm alumina powders. A number of experiments followed involving photoetching under a variety of electrolytes and conditions. After each experiment, the sample was examined using a Hitachi 520D scanning electron microscope. Electrical contact to the microscope table was achieved through the bulk semiconductor material. Image degradation due to charging effects was tolerated to avoid coating the sample with gold.

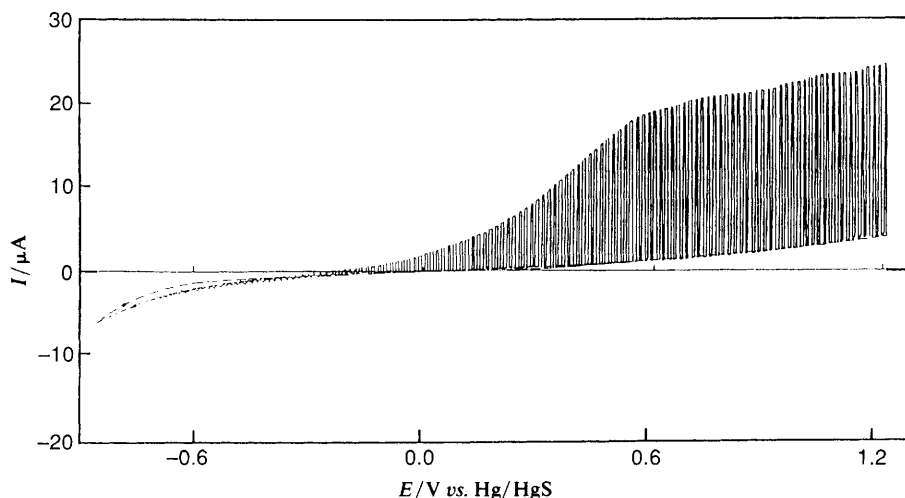


Fig. 1 Photocurrent-voltage curve of n-GaAs in 0.1 mol dm^{-3} KOH- 0.01 mol dm^{-3} Na_2S - 0.01 mol dm^{-3} S obtained with defocused interrupted illumination. The electrode area is $0.09(6) \text{ cm}^2$, electrode potential scan rate 10 mV s^{-1} , and the reference electrode was Hg/HgS in the same solution. Illumination from an HeNe laser, $\lambda = 632.8 \text{ nm}$ of intensity $120 \mu\text{W}$. The potential was scanned from cathodic to anodic voltages, and the dark current is indicated by a broken line

Analytical-grade chemicals were used throughout. Large crystals of Na_2S were washed free of impurities using distilled water and dried with filter paper prior to preparing the polysulfide solution used for the photoetching experiment. Potentials were measured with respect to $\text{Hg}/\text{Hg}_2\text{Cl}_2/1 \text{ mol dm}^{-3}$ KCl in nitrate or alkaline media and Hg/HgS in polysulfide media. The Hg/HgS electrode has a potential $110 \pm 3 \text{ mV}$ vs. $\text{Hg}/\text{Hg}_2\text{Cl}_2/1 \text{ mol dm}^{-3}$ KCl.

Results

The current-voltage curve for n-GaAs in aqueous 0.1 mol dm^{-3} KOH containing polysulfide ion (0.01 mol dm^{-3} Na_2S - 0.01 mol dm^{-3} S) in the dark and under chopped broad-beam illumination is shown in Fig. 1. The power of the incident beam of wavelength 632.8 nm was $120 \mu\text{W}$. A fraction of the GaAs area was photoelectrochemically etched at $+0.7 \text{ V}$ vs. Hg/HgS corresponding to depletion conditions within the space-charge layer. The total current (photocurrent and dark current) and photocurrent image were monitored continuously and simultaneously on a chart recorder and video recorder, respectively. A representative example of the total current response at the onset of photoetching and at longer times when a steady-state etching rate is established is shown in Fig. 2. The sequence of regular pulses indicates a sharp decrease in photocurrent that marks the end of each individual image frame. The transient variation of photocurrent as the beam rasters across the sample during each frame is filtered by the time constant of the recorder which displays an average value. Towards the end of each image cycle the beam moves off the edge of the electrode resulting in the decreasing photocurrent spike. At the start of the etching profile the average photocurrent fluctuates about a slowly increasing background value that becomes stable as surface polishing damage is removed. At much longer times the average photocurrent decreases and becomes constant.

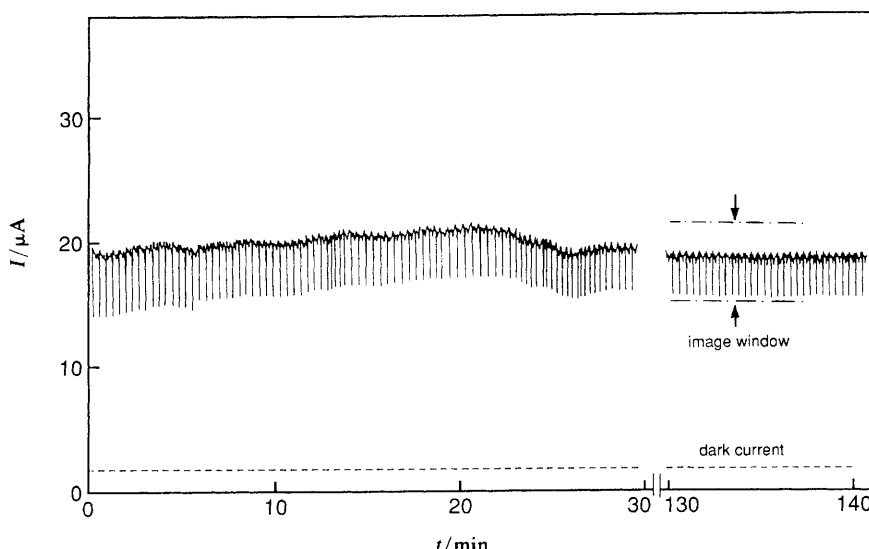


Fig. 2 Current vs. time profile during the photoetching of n-GaAs in 0.1 mol dm^{-3} KOH- 0.01 mol dm^{-3} Na₂S- 0.01 mol dm^{-3} S. The electrode was polarised at +0.7 V vs. Hg/HgS in the same solution. The total electrode area was $0.09(6) \text{ cm}^2$. An area of 0.02 cm^2 was illuminated by rastering a focused beam over the surface ($\lambda = 632.8 \text{ nm}$, $120 \mu\text{W}$). The dark current contribution to the total is indicated by a broken line. The image window indicates the portion of the total current signal that is used to generate the photocurrent image

The total current across the interface was offset after amplification such that only variations in photocurrent across the surface were measured by the image processor instrumentation. This photocurrent window is indicated in Fig. 2 and an example of the photocurrent variation across a single-line scan is shown in Fig. 3. This photocurrent variation was digitised with 8 bit accuracy and displayed as a grey-scale image with white representing a maximum in the photocurrent and black representing a minimum. Photocurrent images corresponding to short and long times into the etching profile are shown in Fig. 4(a) and 4(b). Initially, polishing damage is visible as black line contrast, Fig. 4(a). This contrast disappears from the photocurrent image after ca. $1 \mu\text{m}$ of material has been removed, Fig. 4(b). Three features are distinguished in Fig. 4(b). At the left of the image alternate light and dark horizontal bands of contrast are visible. There are circular patches where the photocurrent is considerably reduced [typified by region A, Fig. 4(b)] and there is a region where the photocurrent is enhanced [region B, Fig. 4(b)]. A comparison with earlier images obtained during the etching profile showed that region B had developed as the etching proceeded.

The photoetched region was examined *ex situ* using a scanning electron microscope and the features observed are shown in Fig. 5. Where the image shows reduced photocurrent in region A, the surface has been etched into a characteristic rippled relief, Fig. 5(a). Where the photocurrent was enhanced, active dissolution has occurred to expose a crack in the surface, Fig. 5(b). The effect of potential on the photocurrent distribution around this crack was evaluated in a separate experiment and these results are shown in Fig. 6. At anodic potentials corresponding to the depletion region of the photocurrent-voltage curve the crack is photoactive, Fig. 6(a). There are also patches in the immediate vicinity where the photoactivity is reduced. As the potential becomes more cathodic, a progressive transition occurs until the charge transfer across the crack is less than that across the adjacent surface, Fig. 6(b) and 6(c). The feature now behaves

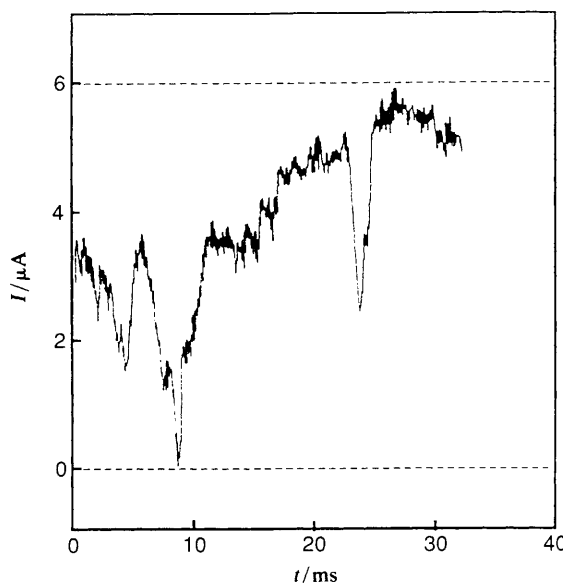


Fig. 3 hotocurrent variation across a single line in the photocurrent image of Fig. 4(b)(CD). The broken lines indicate the bounds of the image window and represent the contrast range, white ($6 \mu\text{A}$) through to black ($0 \mu\text{A}$) offset $25 \mu\text{A}$

as a recombination centre and clearly delineation of this feature will depend markedly on the value of the potential chosen for the photoetching. Prolonged illumination at a potential corresponding to the depletion region develops this feature as shown in the scanning electron micrograph of Fig. 6(d). Preferential etching of specific crystal planes is observed along the sides of the crack. Where the image indicates a reduced photoactivity [centre of Fig. 6(a)] dissolution has not occurred so rapidly and a hillock is visible. Defects with a ripple relief have developed but these have no correspondence with any contrast variation. The groove is caused by prolonged photoetching due to the position of the beam during the line-blanking time. Pitting has appeared on the surface and also on the edge of the groove.

To complete the results in polysulfide media, the formation of a crevice was observed in a separate experiment. This feature is shown in the scanning electron micrograph of Fig. 7(a). The edges of this crevice consist of an array of defects as shown in Fig. 7(b) which developed as a consequence of illumination. The photocurrent image of this region obtained during the growth of the crevice shows clearly that the photocurrent is a maximum at the edges of the crevice and that proliferation of the crevice proceeds by the lateral spreading of the edges of the crevice.

Differences in etching behaviour were also observed depending upon the composition of the solution phase. Photocurrent images in $1 \text{ mol dm}^{-3} \text{ KNO}_3$ in the pH range 1–9 show similar contrast variations as in polysulfide media except that, in addition, local spots of high photoactivity develop, Fig. 8(a). At pH 11 the contrast changes as shown in Fig. 8(b). The photoactive regions remain, but the detailed structure in the contrast disappears. Examination with the scanning electron microscope confirms that damage persists on the surface and that the photoactive regions are caused by dissolution of the substrate with the formation of pits aligned along damage features [Fig. 8(c)]. These pits have a characteristic pattern as shown in Fig. 8(d). Photoetching was also observed in $1 \text{ mol dm}^{-3} \text{ KNO}_3$ at pH 5 and also in $0.1 \text{ mol dm}^{-3} \text{ KOH}$ in the absence of polysulfide species, but scratch lines in particular were not removed. The groove of the scratch is

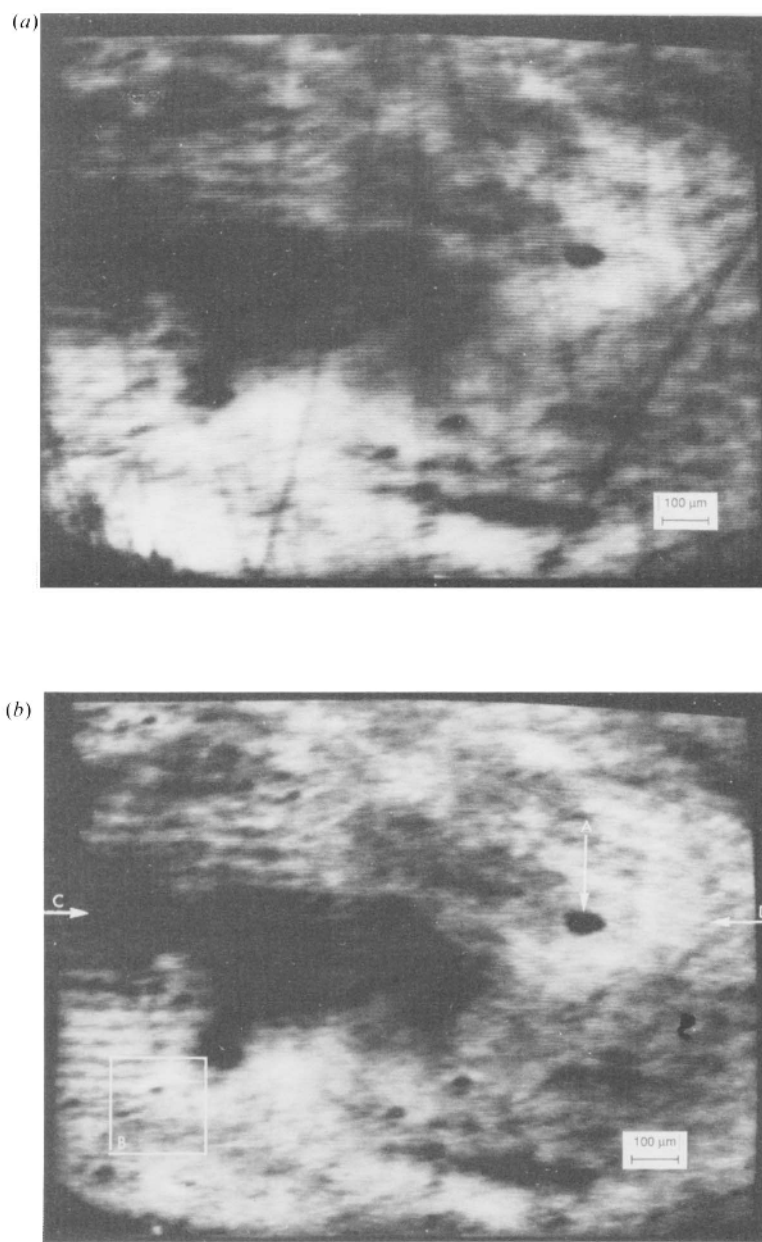
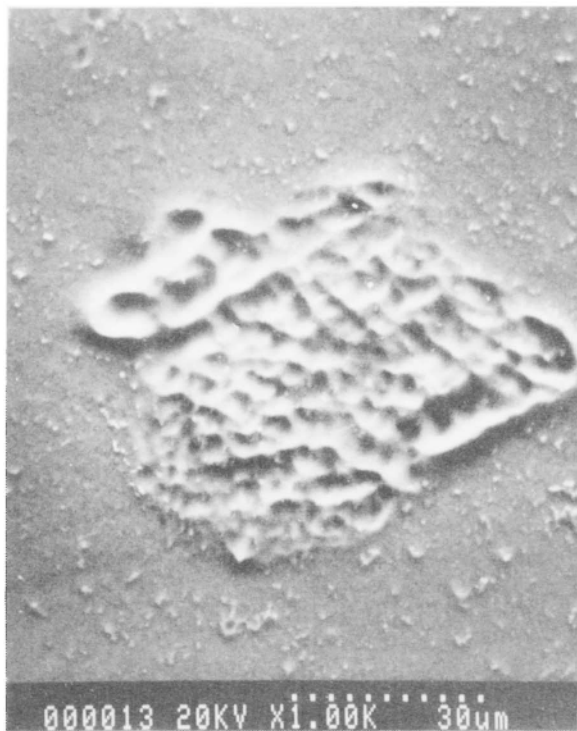


Fig. 4 Photocurrent images n-GaAs in 0.1 mol dm^{-3} KOH- 0.01 mol dm^{-3} Na_2S - 0.01 mol dm^{-3} S at 0.7 V vs. Hg/HgS , (a) at the onset of photoetching and (b) after removal of $1 \mu\text{m}$ of material. An electrode area of 0.02 cm^2 was rastered with focused light from an HeNe laser, $\Lambda = 632.8 \text{ nm}$ of intensity $120 \mu\text{W}$. The scan speed was 31 ms per line from left to right across the image. Contrast variations correspond to a range $0 \mu\text{A}$ (black contrast) through to $6 \mu\text{A}$ (white contrast), offset $25 \mu\text{A}$. White arrows (CD) in (b) indicate the position of the line of data corresponding to Fig. 3 and the regions marked A and B correspond to the micrographs of Fig. 5(a) and (b), respectively

(a)



(b)



Fig. 5 Scanning electron micrographs of an n-GaAs surface after photoetching in 0.1 mol dm^{-3} KOH- 0.01 mol dm^{-3} Na_2S - 0.01 mol dm^{-3} S at 0.7 V vs. Hg/HgS; (a) feature corresponds to the photoinactive region A in Fig. 4(a), and (b) corresponds to photoactive region B

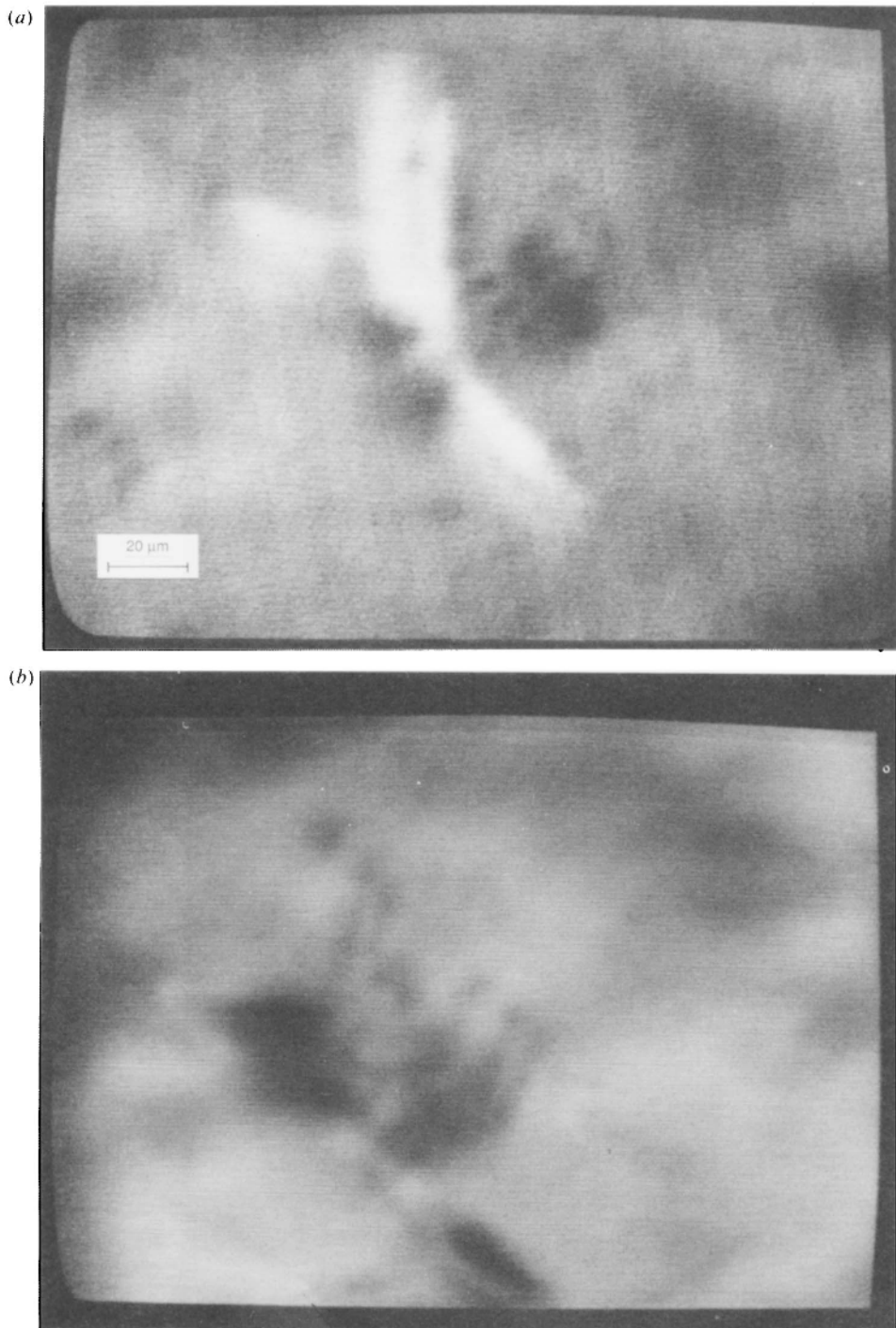
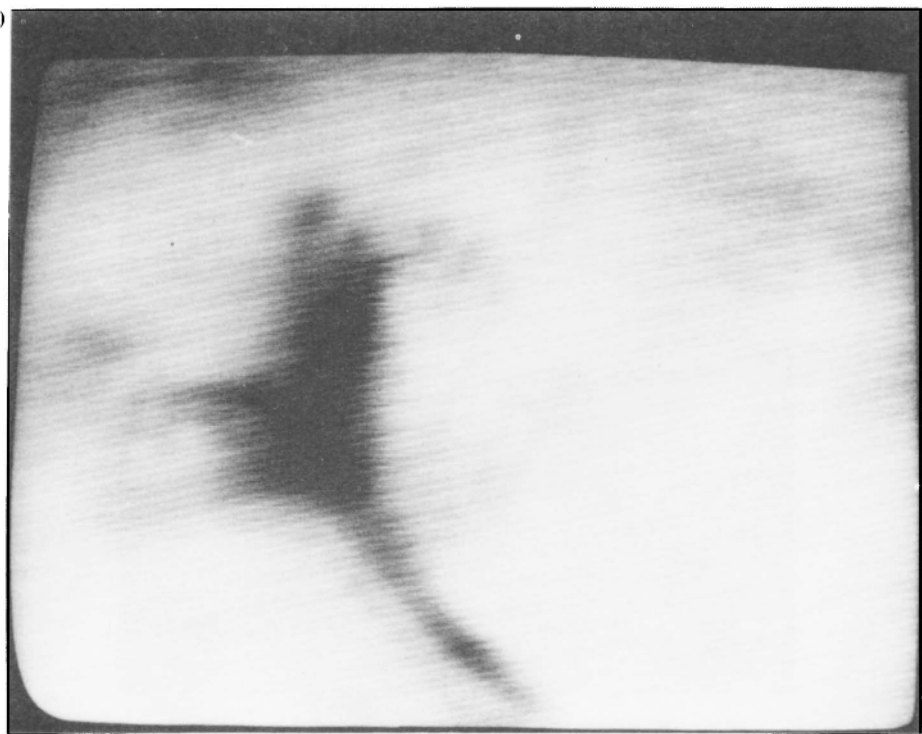


Fig. 6 Effect of potential on the photocurrent distribution in the vicinity of an actively dissolving crack on the surface of n-GaAs in 0.1 mol dm^{-3} KOH- 0.01 mol dm^{-3} Na_2S - 0.01 mol dm^{-3} S. (a) $E = +0.3 \text{ V}$, (b) $E = -0.3 \text{ V}$ and (c) $E = -0.5 \text{ V}$ vs. Hg/HgS in the same solution. (d) Scanning electron micrograph of the crack after imaging (a), (b) and (c). Experimental conditions were as follows; (a) illumination intensity $3.8 \mu\text{W}$, contrast range 50 nA with the black level offset at 300 nA ; (b) illumination intensity $3.8 \mu\text{W}$, contrast range 10 nA with the black level offset at 24 nA ; (c) illumination intensity $38 \mu\text{W}$, contrast range 10 nA with the black level offset at 24 nA ; common parameters are scan speed 32 ms per line , $\lambda = 632.8 \text{ nm}$ and illuminated area $2.7 \times 10^{-4} \text{ cm}^2$; scale as Fig. 6(a)

(c)



(d)



Fig. 6—continued.

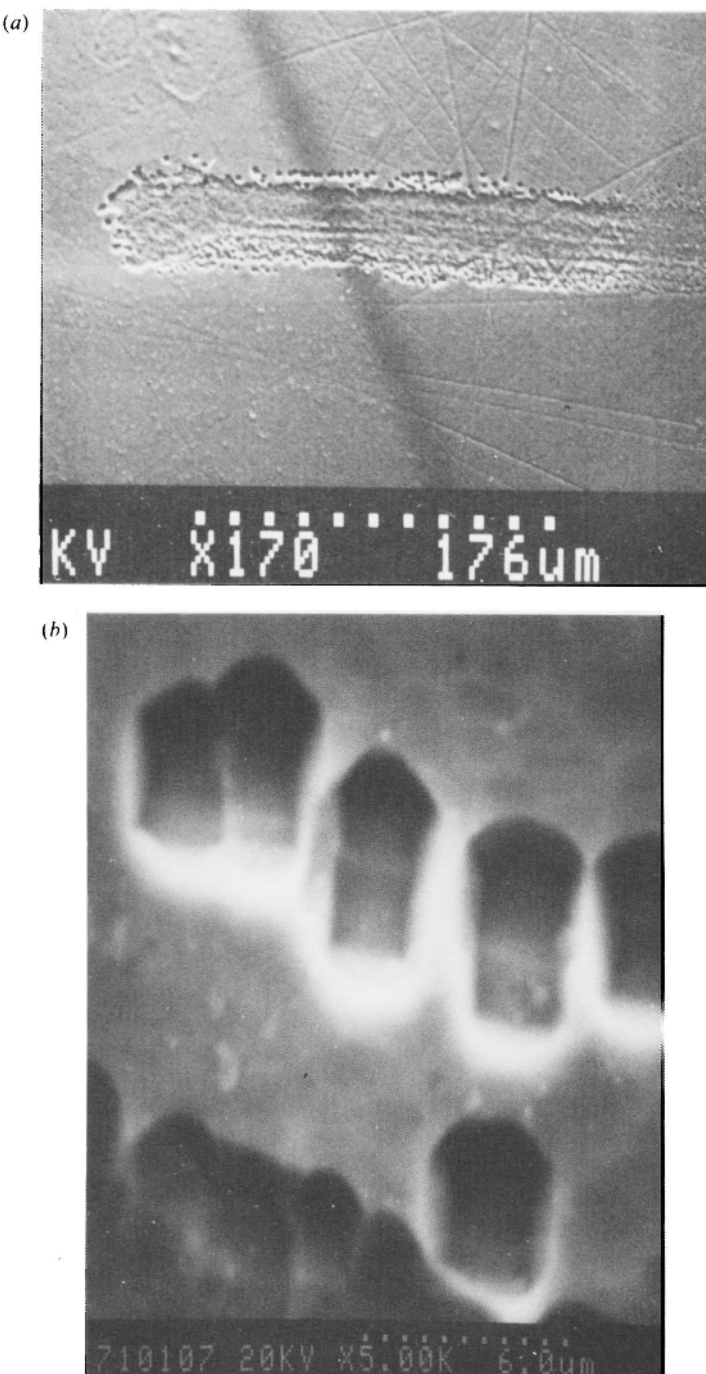


Fig. 7 Photocorrosion of n-GaAs to form a crevice; (a) scanning electron micrograph of the crevice after the photoetching experiment and a close up of the defects bordering the edge of the crevice (b); (c) photocurrent image of the crevice in 0.1 mol dm^{-3} KOH- 0.01 mol dm^{-3} Na_2S - 0.01 mol dm^{-3} S at $E = -0.3 \text{ V}$ vs. Hg/HgS reference electrode, illumination intensity $11 \mu\text{W}$, contrast range 100 nA with black level offset at 140 nA ; the scan speed was 3.0 ms per line , $\lambda = 632.8 \text{ nm}$ and illuminated area $1.2 \times 10^{-3} \text{ cm}^2$

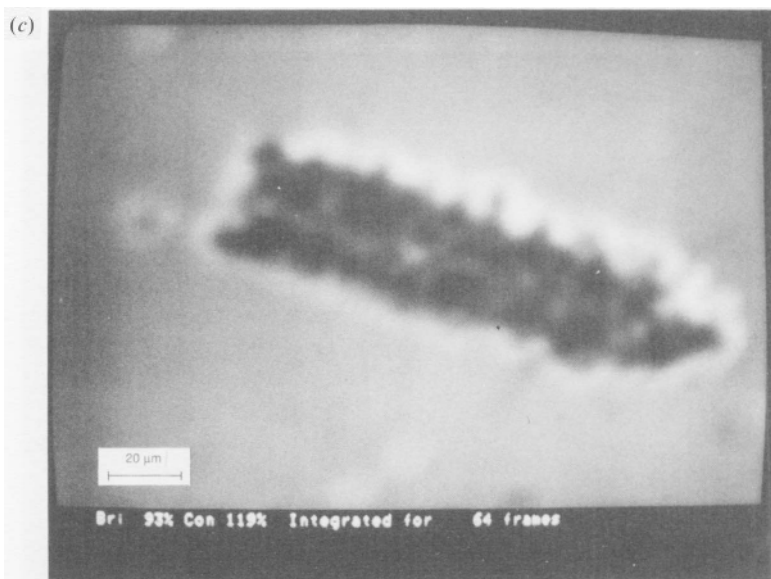


Fig. 7—continued.

etched to create an alignment of elongated ridges with the long axis across the scratch. An example of this feature can also be seen in Fig. 8(d).

These results demonstrate that a combination of *in situ* photocurrent imaging and *ex situ* scanning electron microscopy provides a powerful qualitative tool for examining surfaces. However, there are unexpected difficulties. The photocurrent image of Fig. 9 obtained after *ex situ* examination shows quite clearly circular patches of low photocurrent conversion efficiency that are caused by the impingement of the electron beam. Two mechanisms are suggested, the formation of an oxide film and/or the formation of a carbon film by breakdown of hydrocarbon impurities present in the vacuum chamber of the electron microscope. The effect on the photocurrent image can be removed by a single wipe of the specimen on a wet polishing cloth.

Discussion

The variations in photocurrent that are observed in the images of the interphase can originate through a variety of mechanisms. Two processes can be considered, the generation of the carriers and their subsequent fate. The first process depends upon the band-gap energy, the doping density and the absorption spectrum of the bulk material and, therefore, inhomogeneities in the material composition or the presence of impurity phases will introduce contrast variations reflecting variations in carrier generation rates. Secondly, in order for the photocurrent to be measured in the external circuit, the minority carriers have to move towards the interface and cross the boundary into the solution phase. Clearly, if these carriers are annihilated *en route* by recombination processes within the bulk of the semiconductor or at the interface boundary, or if the electron-transfer process to the electrolyte is impeded by the presence of an insulator film, then the photocurrent will be reduced and again contrast will appear in the image. However, comparison of photocurrent images obtained during a continual photoetching experiment interrupted with scanning electron microscopy allows the effects due to microscopic surface features to be distinguished. Also, bulk inhomogeneities are identified, as they are brought to the surface by the receding interface boundary.

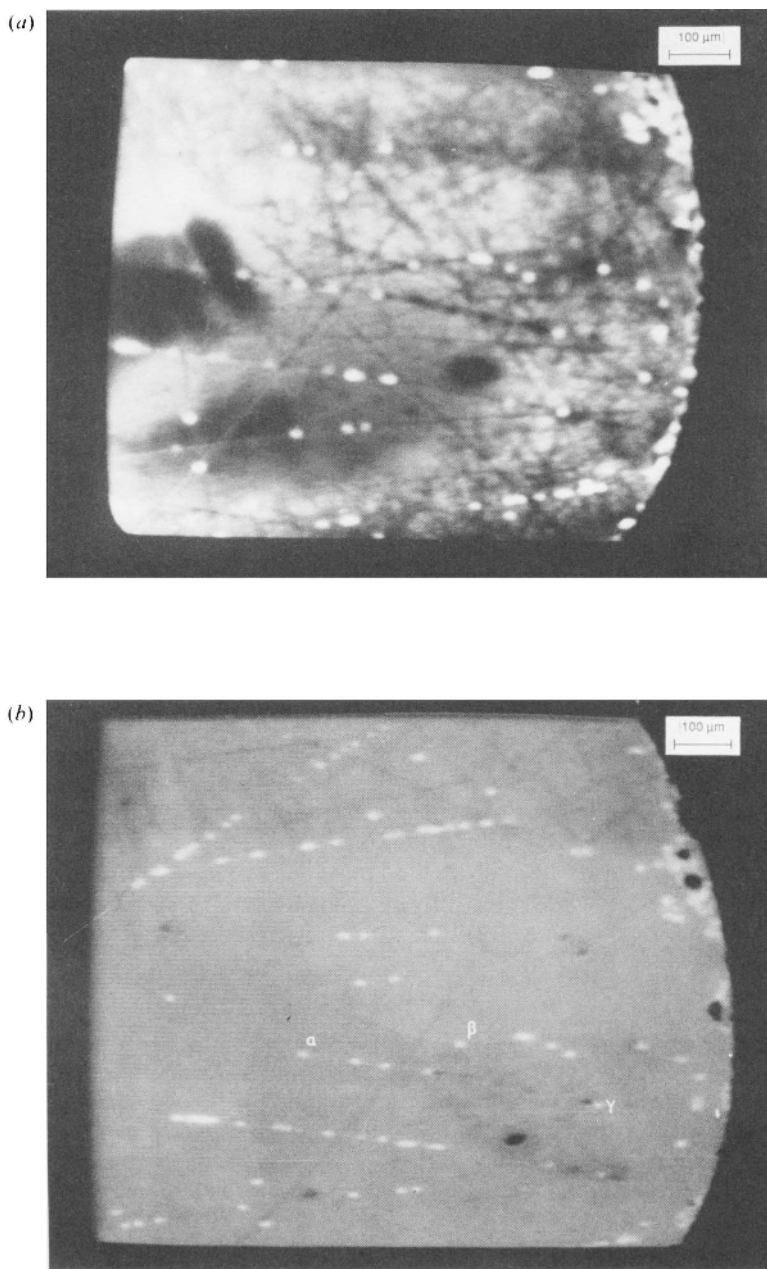


Fig. 8 Photocurrent images of n-GaAs in (a) 1 mol dm^{-3} KNO_3 at pH 5 and (b) after adjusting to pH 11.1 with 0.1 mol dm^{-3} NaOH ; (c) and (d) are scanning electron micrographs of the surface after the photocurrent imaging experiments. Pits labelled α , β and γ align images (b) and (c). (a) Illumination intensity $34 \mu\text{W}$ ($\lambda = 632.8 \text{ nm}$), white contrast represents $10 \mu\text{A}$, black contrast $0 \mu\text{A}$ without offset, scan speed 80 ms per line , potential $-0.5 \text{ V vs. } 1 \text{ mol dm}^{-3}$ calomel. (b) Illumination intensity $34 \mu\text{W}$ ($\lambda = 632.8 \text{ nm}$), white contrast represents $10 \mu\text{A}$, black contrast $0 \mu\text{A}$ without offset, scan speed 10 ms per line , potential $0 \text{ V vs. } 1 \text{ mol dm}^{-3}$ calomel

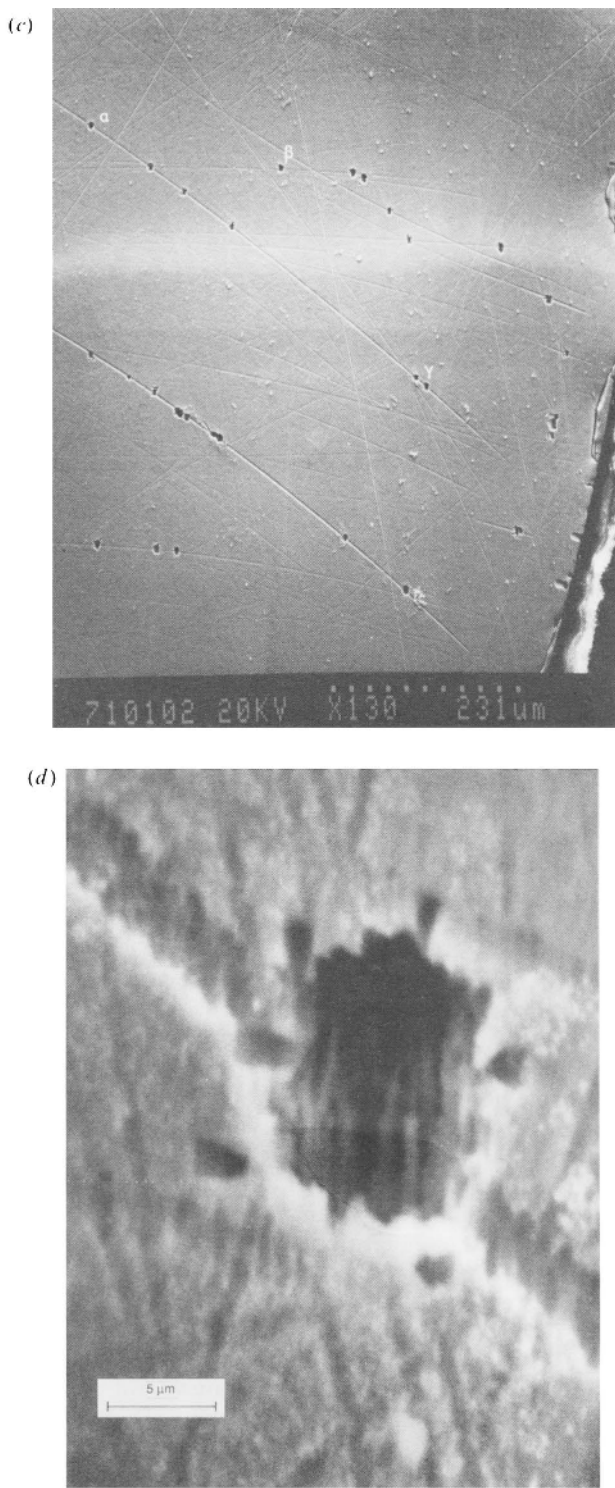


Fig. 8—continued.

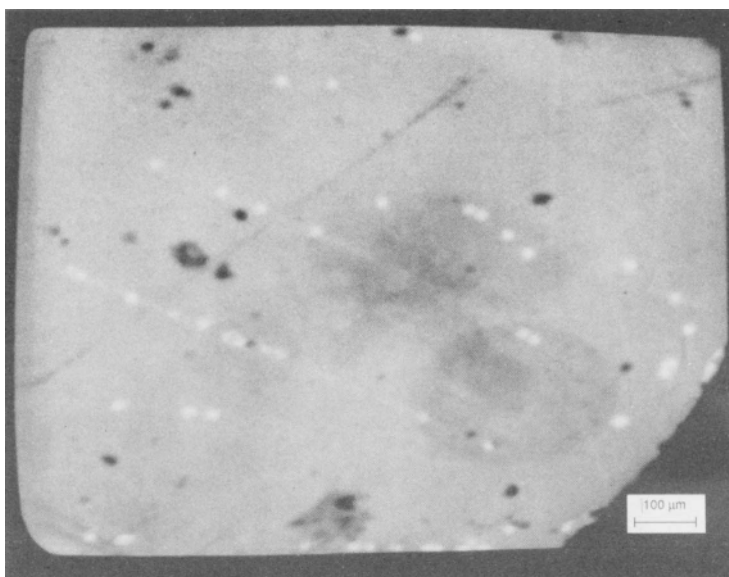


Fig. 9 Photocurrent image of the region shown in Fig. 8(b) after examination of the surface using scanning electron microscopy, dark circles correspond to the regions examined

Consider first the generation rate of the carriers. The reflection coefficient at the GaAs/solution interface calculated from the optical constants of the solid ($n = 3.856$, $k = 0.196$ at $632.8 \text{ nm}^{15,16}$) and the solution ($n = 1.35^{17}$) has a value of 0.23. Correcting the illumination intensity for reflection using this value, and assuming that one electron-hole pair will be generated for each photon absorbed in the solid, implies a theoretical photocurrent of $48 \mu\text{A}$, indicating a photocurrent conversion efficiency of the order of 42% in the depletion region at 0.7 V vs. Hg/HgS . Calculations following the Gartner treatment¹⁸ for a Schottky barrier using the parameters, doping density (N_d) of $1 \times 10^{17} \text{ cm}^{-3}$, absorption coefficient (α) $4 \times 10^4 \text{ cm}^{-1}$, minority carrier diffusion length (L_p) of $2 \times 10^{-5} \text{ cm}$ and relative permittivity (ϵ) of 11, predicts a value of the order of 70% conversion (*i.e.* a plateau current of $34 \mu\text{A}$).

The calculation also indicates that the penetration depth of the light extends well into the bulk solid and, therefore, contrast variations in the photocurrent image will reflect heterogeneity throughout the quasi-neutral region and space-charge region. Much of the mottled background contrast in Fig. 4 is assumed to be due to these effects. This heterogeneity becomes apparent through the carrier generation rate which is extremely sensitive to the parameters N_d and L_p , as shown in Fig. 10. The separation of the effect of these two parameters is difficult at present.

The photocurrent in the plateau originates from carriers that have crossed the solid/electrolyte interface either by substrate dissolution or from capture by the polysulfide species, and the area bounded by successive pulses and the dark current level in Fig. 2 is a measure of the charge passed across the illuminated area that was scanned. Assuming that charge transfer occurs only by photodissolution with the consumption of six holes for each GaAs molecule then the etch rate would be $1.25 \mu\text{m h}^{-1}$ with $5 \mu\text{m}$ depth of material being removed during the experiment. Depth profiling indicates that only $2 (\pm 1) \mu\text{m}$ of material has been removed suggesting that 60% of the charge crossing the interface is captured by the polysulfide species. This contrasts with a study on the photoelectrochemical etching of an MBE-grown GaAs δ -doped structure¹⁹ of known layer thickness which showed hole capture by the polysulfide accounting for more than

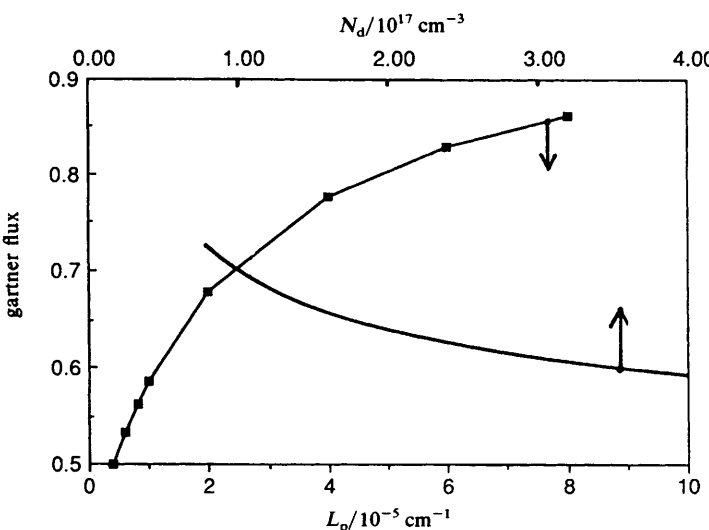


Fig. 10 Model calculation of the theoretical carrier generation rate normalised to the incident photon flux showing the sensitivity to changes in the doping density and the minority carrier diffusion length. Parameters are $\epsilon = 11$, $N_d = 1.3 \times 10^{17} \text{ cm}^{-3}$, $\alpha = 4 \times 10^4 \text{ cm}^{-1}$, $L_p = 2 \times 10^{-5} \text{ cm}$ and the space-charge potential is 2.0 V unless otherwise stated

99% of the total photocurrent. In summary, these rough calculations imply that 50% of the carriers generated are lost through recombination processes either in the bulk or on the surface, 30% are captured by the redox couple and 20% consume the substrate.

This high loss through recombination is to be expected and it is assumed that variations in the recombination rate are the main cause of image contrast: the sample had not been chemically etched to remove damage from the surface region and the GaAs was poor-quality material compared with modern material grown using molecular-beam epitaxy, as it contained bulk impurities in the form of doping striations, precipitates and crystallographic defects, as well as preparation damage features.^{1,2,20} The alternate light and dark banding on the left of Fig. 4(b) is attributed to striation doping: *i.e.* impurity (dopant) variations due to thermal oscillations in the vicinity of the freezing interface during crystal growth. The feature characterised by the ripple type of relief is probably a precipitate, Fig. 5(a). The area of surface that it occupies shows no photocurrent contrast, suggesting that the material is foreign and not absorbing at the energy of the incident beam. The feature B in Fig. 5(b) is a crack in the bulk of the material that has been exposed by the receding surface. The photoactive regions in Fig. 6(a) are due to the preferential dissolution of specific crystal planes. These planes become clearly defined after prolonged etching as seen in Fig. 6(d). Pits are formed under conditions of high photon flux [Fig. 6(d)] or when charge transfer is impeded by the presence of a passivating layer, as, for example, in KNO_3 solutions at intermediate pH values. They are highly photoactive because the substrate is rapidly dissolving at the pit. The second example of contrast due to crystallographic defects is the formation of the crevice in Fig. 7.

Mechanical damage features initially show as photoinactive regions in the polysulfide electrolyte but these disappear rapidly from the image contrast although they are still visible optically, Fig. 4. This is not observed in the KNO_3 and KOH electrolytes. In these media elongated pits were formed. It has been reported previously that certain chemical etches delineate surface scratches as close packed or separated lines of pits

all elongated along the $\langle 100 \rangle$ direction.¹ These pits have sharp-edged bottoms and have been termed 'boat pits'. The presence of boat pits is an indication of work damage present at the surface, but the specific defects which develop into boat pits are not known. In a separate study these features were termed 'long microcavities' and were claimed to be due to etching of either dislocation loops or stacking faults. The rapid loss of contrast in the photocurrent image at the damage features in the presence of polysulfide implies that the defects responsible for the pits, or at least the environment in the vicinity of the damage, are specific for the adsorption of polysulfide, which then stabilises any further development of the features.

Still elusive from these photocurrent images is the surface state. The form of the photocurrent-voltage curve as shown in Fig. 1 differs substantially from the expected behaviour for an ideal Schottky barrier. The flat-band potential in the dark in 0.1 mol dm⁻³ KOH is at -1.75 V vs. SCE and is unaffected by the addition of polysulfide species.²¹ Although the observed flat-band potential shifts anodically with increasing illumination, the value saturates at -1.55 V, so there is a considerable onset potential before photocurrent is observed. It is in this anomalous region that recombination processes dominate. While there are subtle changes in the contrast surrounding macroscopic defects at potentials within the recombination region, the contrast variations across the background surface change little, Fig. 6. The image appears as if it has been attenuated. A detailed study of the properties of the recombination region using intensity-modulated photocurrent spectroscopy concluded that the surface stoichiometry of n-GaAs changes in such a way that a gallium-rich surface forms at negative potentials, whereas As accumulates at positive potentials until As^{III} dissolution occurs, whereupon the response tends to follow the predictions of the Schottky barrier model.²¹ Distinct regions of image contrast are, however, not observed for potentials within the range where recombination processes dominate the photocurrent. The conclusion is that the surface state and/or metal-enriched surface has both a dimension and an average spacing smaller than the beam width; that is, a very large number of very small recombination centres causes the overall diminution in conversion efficiency.

The resolution of the images is less than is expected with a focused beam of 3–4 μm diameter and poorer than an image obtained on a solid-state junction.²² The resolution in the electrochemical system depends upon the spatial distribution of the photogenerated carriers as they arrive at the interface and also on the kinetics of charge transfer. A theoretical calculation of carrier transport to the surface in the semiconductor space-charge region has been made for a Gaussian beam profile.²³ For a spot size diameter of 2.6 μm the radial distribution of carriers at the surface was 8 μm and >20 μm for doping densities 10^{18} and 10^{16} cm⁻³, respectively. Resolution should therefore increase with the more doped materials and also with increasing energetic illumination as the penetration depth of the light is compressed.^{24,25} At high laser intensities where etch-rate saturation occurs owing to kinetic limitations, the etched groove exhibits a flattened bottom with a greater width than the beam width.²³ This etching profile can be seen in Fig. 6(d) across the groove corresponding to the position of the focused beam during the line-blanking period. The width of the groove, 20 μm , is comparable with the results of the above calculations and the Gaussian profile is seen on the edges of the trough. At the electrolyte junction, fast charge transfer is important to remove the holes arriving at the surface, otherwise an excess charge will accumulate in the illuminated zone and the bands will straighten locally and a lateral photovoltage will be established. The lateral migration of carriers has not been included in the above calculations but will add to the general broadening of the carrier distribution. In practice, the resolution improves at lower illumination intensities but, of course, there is a trade off as the signal-to-noise ratio also decreases. Finally, in the direct imaging mode, the transient behaviour to chopped illumination will also degrade the resolution at potentials corresponding to the recombination region. The scanned experiment is equivalent to a

chopped-light experiment because the signal at any point on the surface is the sum of the photocurrent on the newly illuminated area plus any transient contribution due to the previous illuminated area returning to its dark steady-state condition. The edge resolution will be degraded by the transient time constant and will improve at lower scan velocities. This prediction has been confirmed in many of the systems studied. Transient effects predominate when the line scan speed is comparable with the transient time constant.

In conclusion, results are presented that show directly, in a qualitative way, the distribution of interfacial charge transfer in the vicinity of microscopic surface defects and the effect of potential and electrolyte composition on this distribution.

Financial support for this work was provided by the Underlying Science Programme of the United Kingdom Atomic Energy Authority.

References

- 1 D. J. Stirland and B. W. Straughan, *Thin Solid Films*, 1976, **31**, 139.
- 2 B. Tuck, *J. Mater. Sci.*, 1975, **10**, 321.
- 3 M. M. Faktor and J. L. Stevenson, *J. Electrochem. Soc.*, 1978, **125**, 621.
- 4 M. A. Butler, *J. Electrochem. Soc.*, 1983, **130**, 2385.
- 5 M. A. Butler, *J. Electrochem. Soc.*, 1984, **131**, 2185.
- 6 D. Shukla, T. Wines and U. Stimming, *J. Electrochem. Soc.*, 1987, **134**, 2086.
- 7 P. S. Tyler, M. R. Kozlowsky, W. H. Smyrl and R. T. Atanasoski, *J. Electrochem. Soc.*, 1987, **237**, 295.
- 8 D. E. Williams, A. M. Riley and R. Peat, *Proc. SPIE*, 1987, **809**, 44.
- 9 R. Peat, A. J. Kucernak, D. E. Williams and L. M. Peter, *Semicond. Sci. Technol.*, 1990, **5**, 914.
- 10 R. Peat, A. J. Kucernak and D. E. Williams, *Electrochim. Acta*, 1992, **5**, 933.
- 11 G. Razzini and L. Peraldo Bicelli, B. Scrosati, P. Salvador, M. Pujadas and F. Decker, *J. Electrochem. Soc.*, 1988, **135**, 1934.
- 12 G. Vercruyse, W. Rigole and W. P. Gomes, *Solar Energy Mater.*, 1985, **12**, 157.
- 13 R. Peat, A. Riley and D. E. Williams, *J. Electrochem. Soc.*, 1989, **136**, 3352.
- 14 A. R. J. Kucernak, R. Peat and D. E. Williams, *Electrochim. Acta*, 1992, in the press.
- 15 *Handbook of Optical Constants of Solids*, ed. E. D. Palik, Academic Press, London, 1985.
- 16 H. C. Casey Jr., D. D. Sell and K. W. Wecht, *J. Appl. Phys.*, 1975, **46**, 250.
- 17 *Handbook of Chemistry and Physics*, CRC Press, Boca Raton, FL, 55th edn., 1974.
- 18 W. W. Gartner, *Phys. Rev.*, 1959, **116**, 84.
- 19 A. R. J. Kucernak, R. Peat, D. E. Williams, J. H. Wolter, P. M. Koenraad and M. Leys, 1992, submitted.
- 20 A. Yamamoto and S. Yano, *J. Electrochem. Soc.*, 1975, **122**, 260.
- 21 J. Li and L. M. Peter, *J. Electroanal. Chem.*, 1986, **199**, 1.
- 22 P. F. Fontein, P. Hendriks, J. Wolter, A. R. Kucernak, R. Peat and D. E. Williams, *Semicond. Sci. Technol.*, 1989, **4**, 837.
- 23 M. N. Ruberto, X. Zhang, R. Scarmozzino, A. E. Wilner, D. V. Podlesnik and R. M. Osgood Jr., *J. Electrochem. Soc.*, 1991, **138**, 1174.
- 24 F. W. Ostermayer Jr., P. A. Kohl and R. M. Lum, *J. Appl. Phys.*, 1985, **58**, 4390.
- 25 M. M. Carrabba, N. M. Nguyen and R. D. Rauh, *J. Electrochem. Soc.*, 1987, **134**, 1855.